

**s-wave superconductivity in kagome metal CsV_3Sb_5 revealed by
 $^{121/123}\text{Sb}$ NQR and ^{51}V NMR measurements**

Chao Mu,^{1,2} Qiangwei Yin,³ Zhijun Tu,³ Chunsheng
Gong,³ Hechang Lei,³ Zheng Li,^{1,2,*} and Jianlin Luo^{1,2,4,†}

¹*Beijing National Laboratory for Condensed Matter Physics and Institute of Physics,
Chinese Academy of Sciences, Beijing 100190, China*

²*School of Physical Sciences, University of Chinese
Academy of Sciences, Beijing 100190, China*

³*Department of Physics and Beijing Key Laboratory of
Opto-electronic Functional Materials & Micro-nano Devices,
Renmin University of China, Beijing 100872, China*

⁴*Songshan Lake Materials Laboratory, Dongguan 523808, China*

Abstract

We report $^{121/123}\text{Sb}$ nuclear quadrupole resonance (NQR) and ^{51}V nuclear magnetic resonance (NMR) measurements on kagome metal CsV_3Sb_5 with $T_c = 2.5$ K. Both ^{51}V NMR spectra and $^{121/123}\text{Sb}$ NQR spectra split after a charge density wave (CDW) transition, which demonstrates a commensurate CDW state. The coexistence of the high temperature phase and the CDW phase between 91 K and 94 K manifests that it is a first order phase transition. At low temperature, electric-field-gradient fluctuations diminish and magnetic fluctuations become dominant. Superconductivity emerges in the charge order state. Knight shift decreases and $1/T_1T$ shows a Hebel-Slichter coherence peak just below T_c , indicating that CsV_3Sb_5 is an s-wave superconductor.

Kagome lattice has been intensely studied in condensed matter physics due to its geometric frustration and nontrivial band topology. Depending on the electron filling, on-site repulsion U , and nearest-neighbor Coulomb interaction V , several possible states have been proposed as the ground state[1, 2], such as quantum spin liquid[3–5], charge density wave (CDW)[6], and superconductivity[7, 8].

Recently, superconductivity was discovered in the kagome metal $AV_3\text{Sb}_5$ ($A = \text{K, Rb, Cs}$), which undergoes a CDW transition before the superconducting transition[9–12]. Scanning tunneling microscopy (STM) observed a chiral charge order that breaks time-reversal symmetry[13] and leads to the anomalous Hall effect in the absence of magnetic local moments[14–17]. This chiral charge order is energetically preferred and tends to yield orbital current[18]. Inelastic x-ray scattering and Raman scattering exclude strong electron-phonon coupling driven CDW[19], while optical spectroscopy supports that CDW is driven by nesting of Fermi surfaces[20]. High pressure can suppress CDW transition and reveal a superconducting dome in the P - T phase diagram[21, 22]. Further increasing pressure, a new superconducting phase emerges[23–25].

STM studies observed possible Majorana modes[26] and pair density wave[27], which points to unconventional superconductivity in the surface state. Signatures of spin-triplet pairing and an edge supercurrent have been observed in $\text{Nd}/\text{K}_{1-x}\text{V}_3\text{Sb}_5$ devices[28]. Whether the exotic surface superconducting state is intrinsic or comes from heterostructures, such as $\text{Bi}_2\text{Te}_3/\text{NbSe}_2$ [29], needs to clarify the gap symmetry in the bulk state first. Thermal

* lizheng@iphy.ac.cn

† jlluo@iphy.ac.cn

conductivity measurements on CsV_3Sb_5 down to 0.15 K showed a finite residual linear term, which suggests a nodal gap and points to unconventional superconductivity[25]. On the other hand, magnetic penetration depth of CsV_3Sb_5 measured by tunneling diode oscillator showed a clear exponential behavior at low temperatures, which provides an evidence for nodeless superconductivity but does not rule out fully-gapped unconventional superconductivity[30].

In this work, we report nuclear magnetic resonance (NMR) and nuclear quadrupole resonance (NQR) investigations on CsV_3Sb_5 . The splitting of ^{51}V spectra and $^{121/123}\text{Sb}$ spectra demonstrates that a commensurate CDW order forms at 94 K with a first-order transition and coexists with superconductivity. In the superconducting state, Knight shift decreases and a Hebel–Slichter coherence peak appears in the spin-lattice relaxation rate just below T_c , which provides evidences for s-wave superconductivity in CsV_3Sb_5 .

Single crystals of CsV_3Sb_5 were synthesized using the self-flux method, as reported in Ref.[21]. Superconductivity with $T_c = 2.5$ K is confirmed by dc magnetization measured using a superconducting quantum interference device (SQUID). The NMR and NQR measurements were performed using a phase coherent spectrometer. The spectra were obtained by frequency step and sum method which sums the Fourier transformed spectra at a series of frequencies[31]. The spin-lattice relaxation time T_1 was measured using a single saturation pulse.

Figure 1 (a) shows the spectra of ^{51}V with $\mu_0 H (= 8.65 \text{ T}) \parallel c$. ^{51}V with $I = 7/2$ has seven NMR peaks at 150 K. Below $T_{\text{CDW}} = 94$ K, the magnitude of original peaks decreases gradually and two sets of new peaks arise, which indicates that the CDW transition is commensurate and there are two different sites of V atoms in the CDW state. The coexistence of two phases between 91 K and 94 K demonstrates that the CDW transition is of first-order due to a simultaneous superlattice transition[10]. The quadrupole resonance frequencies of both ^{51}V sites increase with decreasing temperature below 94 K, as shown in Fig. 1 (b).

Knight shift ^{51}K is deduced from the central peaks and is summarized in Fig. 1 (c). Below T_{CDW} , two splitting peaks give two Knight shift values, one of which jumps up and the other jumps down. The corresponding $^{51}(1/T_1T)$ jumps to the opposite side or does not change at T_{CDW} , as shown in Fig. 1 (d). We also measured Knight shift and $^{51}(1/T_1T)$ the with $H \perp c$, as shown in Fig S1 of the Supplemental Material, which also shows an opposite trend at T_{CDW} . Therefore, the splitting of ^{51}K is not caused by different hyperfine couplings,

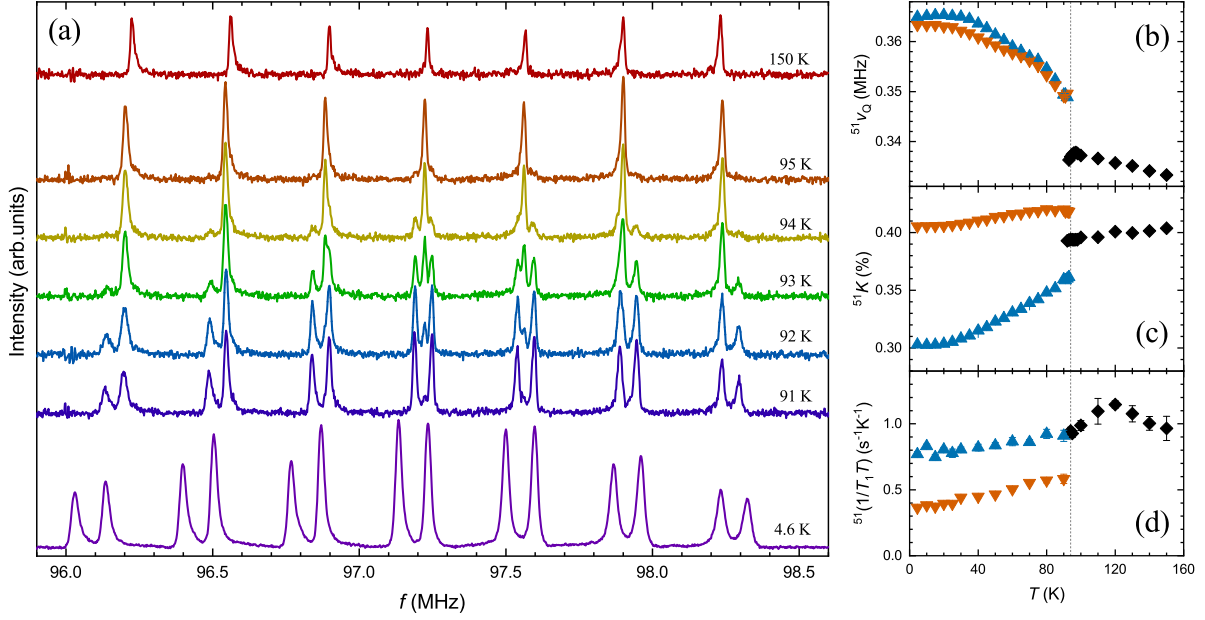


FIG. 1. (a) ^{51}V -NMR spectra with $H \parallel c$. (b) Temperature dependence of quadrupole resonance frequency ν_Q . (c) Temperature dependence of the Knight shift of ^{51}V . (d) Temperature dependence of the $^{51}(1/T_1T)$ measured at the central peaks. The vertical dashed line indicates the position of T_{CDW} .

but by the change of the orbital part of Knight shift.

$^{51}(1/T_1T)$ in a Fermi liquid state is proportional to the square of the density of states (DOS) around the Fermi energy $N(E_F)$. Just below T_{CDW} , $^{51}(1/T_1T)$ of the right peak jumps to 64% of the value above T_{CDW} , indicative of the decrease of $N(E_F)$ by 20%. $^{51}(1/T_1T)$ of the left peak is smooth at T_{CDW} . The difference of $^{51}(1/T_1T)$ between two V sites manifests the modulation of DOS at different V positions, which is consistent with 2×2 CDW charge order[27]. ^{51}V has a very small quadrupole moment, $Q = -5.2 \times 10^{-30} \text{ m}^2$. Therefore, the relaxation is governed by magnetic fluctuations and can reflect the change in the DOS, even though the electric field gradient (EFG) fluctuates strongly near T_{CDW} . On the contrary, ^{121}Sb and ^{123}Sb have larger quadrupole moments, $^{121}Q = -54.3 \times 10^{-30} \text{ m}^2$ and $^{123}Q = -69.2 \times 10^{-30} \text{ m}^2$ respectively, which can be used to detect the EFG fluctuations and perform NQR measurement.

In order to study the superconducting state, we must perform measurement at a magnetic field lower than the upper critical field, $\mu_0 H_{c2} \sim 0.5 \text{ T}$ [25]. Usually NQR experiments do

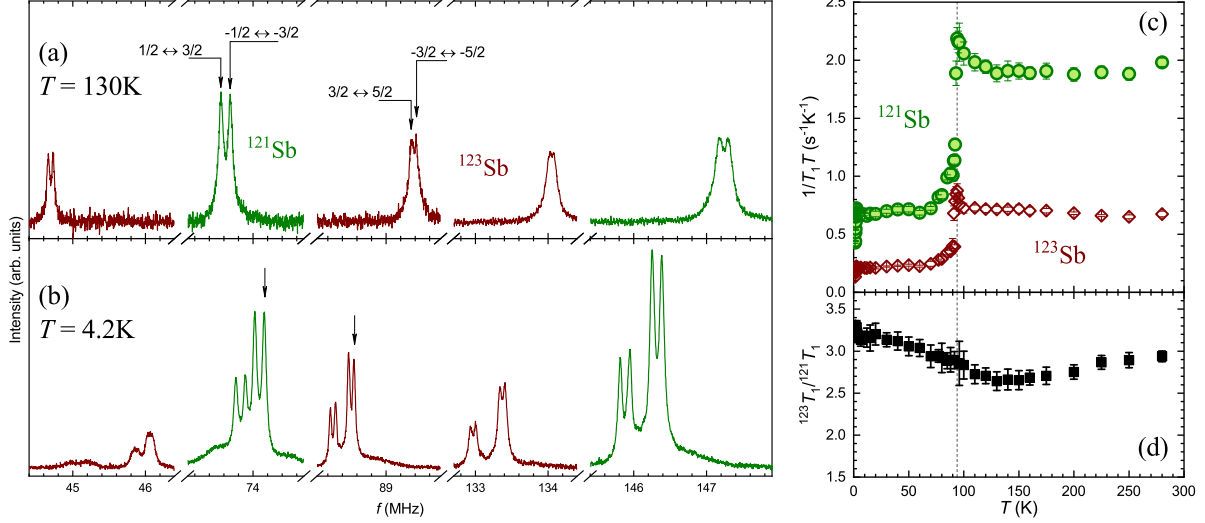


FIG. 2. $^{121/123}\text{Sb}$ -NQR spectra with a perturbing field of 64 Oe along c -axis at (a) 130 K and (b) 4.2 K, respectively. The arrows mark the peaks where T_1 was measured. (c) Temperature dependence of the $1/T_1T$ measured with ^{121}Sb at $-1/2 \leftrightarrow -3/2$ peak and ^{123}Sb at $-3/2 \leftrightarrow -5/2$ peak, respectively. (d) Temperature dependence of the $^{121/123}\text{Sb}$ isotopic ratio $^{123}T_1/^{121}T_1$. The vertical dashed line indicates the position of T_{CDW} .

not need applying magnetic field, however Knight shift cannot be measured at zero field. Here we measure ^{121}K by applying a perturbing field of 64 Oe that is larger than the lower critical field, $\mu_0 H_{c1} \sim 2 \text{ mT}$ [32]. With a perturbing field, the nuclear spin Hamiltonian is the sum of electric quadrupole interactions and the nuclear Zeeman energy[33]

$$\begin{aligned}
 \mathcal{H} &= \mathcal{H}_Q + \mathcal{H}_Z \\
 &= \frac{h\nu_{zz}}{6} \left[(3I_z^2 - I^2) + \frac{\eta(I_+^2 + I_-^2)}{2} \right] \\
 &\quad - \gamma\hbar(1+K)H_0 \left(I_z \cos\theta + \frac{I_+ e^{-i\phi} + I_- e^{i\phi}}{2} \sin\theta \right)
 \end{aligned} \tag{1}$$

where ν_{zz} is the quadrupole resonance frequency along the principal axis (c -axis), $\nu_{zz} \equiv \frac{3e^2qQ}{2I(2I-1)}$, with $eq = V_{zz}$. η is an asymmetry parameter of the EFG, $\eta = \frac{V_{xx} - V_{yy}}{V_{zz}}$. V_{xx} , V_{yy} , V_{zz} are the EFGs along the x , y , z directions respectively. θ and ϕ are the polar and azimuthal angles between the direction of the applied field and the principal axis of EFG. When η is small enough to be negligible, the resonance frequency at a small perturbation field along c -axis is

$$\nu_{\text{NQR}}(H_0) = \nu_{\text{NQR}}(0) \mp \gamma(1+K)H_0, \quad I_z = \pm|I_z| \tag{2}$$

The perturbing field eliminates the degeneration of $\pm I_z$ and results in a spectra splitting. When $H_0 \perp c$, the peak of $|\pm\frac{1}{2}\rangle \leftrightarrow |\pm\frac{3}{2}\rangle$ is split by the perturbing field, while other peaks are not affected[34].

$$\begin{aligned} \nu_{\text{NQR}}(H_0) &= \nu_{\text{NQR}}(0) \pm \frac{I + \frac{1}{2}}{2} \gamma(1 + K)H_0, \quad |\pm\frac{1}{2}\rangle \leftrightarrow |\pm\frac{3}{2}\rangle \\ \nu_{\text{NQR}}(H_0) &= \nu_{\text{NQR}}(0), \quad |\pm m\rangle \leftrightarrow |\pm(m + 1)\rangle, \quad m \geq \frac{3}{2} \end{aligned} \quad (3)$$

where m is a half-integer.

There are two isotopes of Sb nuclei which are ^{121}Sb with $I = 5/2$ and ^{123}Sb with $I = 7/2$. The NQR spectra should contain two ^{121}Sb peaks and three ^{123}Sb peaks. Figures 2 (a) and 2(b) show the spectra with a perturbing field of 64 Oe along c -axis, which eliminates the degeneration of $\pm I_z$ and results in a small spectral splitting. There are two different crystallographic sites for Sb in CsV_3Sb_5 with the atomic ratio of $\text{Sb1} : \text{Sb2} = 1 : 4$ [9]. The relative intensities of different sites are proportional to their atomic ratio[35], so Sb2 site has larger spectral intensity than Sb1 site. The spectra in Figs. 2 (a) and 2 (b) are of Sb2 atoms which encapsulate the kagome layer with a graphite-like network. Sb1 atoms located in the kagome plane with V atoms have weak spectra, which are presented in the Supplemental Material. The ν_{zz} and η deduced from the spectra above and below T_{CDW} are summarized in Table I, where η is zero above T_{CDW} reflecting isotropy in the xy -plane. Below T_{CDW} , η of Sb2 changes to finite values, which indicate the breaking of in-plane symmetry and two unequal sites of Sb2 with the ratio of 1 : 2. The slightly decreasing ν_{zz} implies that the main change is not the EFG strength, but the EFG direction at Sb2 sites. On the other hand, the EFG at Sb1 site changes frequency obviously without asymmetry.

T_1 was measured at $|\frac{1}{2}\rangle \leftrightarrow |\frac{3}{2}\rangle$ peak of $^{121}\text{Sb2}$ and $|\frac{3}{2}\rangle \leftrightarrow |\frac{5}{2}\rangle$ peak of $^{123}\text{Sb2}$ respectively.

TABLE I. The quadrupole resonance frequencies and asymmetry parameters.

T	site	η	$^{121}\nu_{zz}$	$^{123}\nu_{zz}$
130 K	Sb1	0	71.41	43.35
	Sb2	0	73.62	44.69
4.2 K	Sb1	0	78.19	47.16
	Sb2'	0.097	73.08	44.36
	Sb2''	0.099	73.31	44.50

After spectra splitting below T_{CDW} , T_1 was measured at the right-side peaks, marked by arrows in Fig. 2 (b). The degeneration is eliminated by the magnetic field, so the NQR recovery curves are no longer applicable. The recovery curve used for $|-1/2\rangle \leftrightarrow |-\frac{3}{2}\rangle$ transition of ^{121}Sb is

$$1 - \frac{M(t)}{M(\infty)} = \frac{1}{35}e^{-\frac{t}{T_1}} + \frac{3}{56}e^{-\frac{3t}{T_1}} + \frac{1}{40}e^{-\frac{6t}{T_1}} + \frac{25}{56}e^{-\frac{10t}{T_1}} + \frac{25}{56}e^{-\frac{15t}{T_1}} \quad (4)$$

The recovery curve used for $|-3/2\rangle \leftrightarrow |-\frac{5}{2}\rangle$ transition of ^{123}Sb is

$$1 - \frac{M(t)}{M(\infty)} = \frac{1}{84}e^{-\frac{t}{T_1}} + \frac{1}{21}e^{-\frac{3t}{T_1}} + \frac{1}{132}e^{-\frac{6t}{T_1}} + \frac{25}{308}e^{-\frac{10t}{T_1}} + \frac{100}{273}e^{-\frac{15t}{T_1}} + \frac{49}{132}e^{-\frac{21t}{T_1}} + \frac{49}{429}e^{-\frac{28t}{T_1}} \quad (5)$$

We use the same fitting function for both above and below T_{CDW} , since the η is small. Figure 2 (c) shows the temperature dependence of $1/T_1T$ of $^{121/123}\text{Sb}$. Upon cooling, $^{121/123}(1/T_1T)$ starts to increase a little and drops sharply below T_{CDW} for both ^{121}Sb and ^{123}Sb . With further cooling, $^{121/123}(1/T_1T)$ becomes constant from 70 K to T_c , which obeys the Korringa relation and suggests that the system is in a Fermi liquid state. $^{51}(1/T_1T)$ of ^{51}V has shown that DOS loss is only 20%. Here the large drop implies that the EFG fluctuations play an important role above T_{CDW} and are suppressed after CDW transition. Moreover, $^{121/123}(1/T_1T)$ decreases continuously without sudden jump like $^{51}(1/T_1T)$. This implies that the superlattice transition has strong effect on V atoms that locate in the kagome plane, but has very small effect on Sb2 atoms that locate outside the kagome plane. Therefore, $^{121/123}(1/T_1T)$ of Sb2 shows a second-order CDW transition behavior.

In general, a spin-lattice relaxation occurs through magnetic and/or electric-quadrupole channels. The magnetic relaxation is related to the gyromagnetic ratio γ_n and gives $^{123}T_1/^{121}T_1 = 3.4$, while the electric-quadrupole relaxation is related to the quadrupole moment Q and gives $^{123}T_1/^{121}T_1 = 1.5$ [36]. Above T_{CDW} , $^{123}T_1/^{121}T_1$ is smaller than 3, as shown in Fig. 2 (d), which indicates that both magnetic fluctuations and EFG fluctuations are important. Below T_{CDW} , the ratio increases with decreasing temperature and approaches to 3.4 at zero temperature limit, which indicates that the magnetic process becomes dominant at low temperature. Therefore, the effect of EFG fluctuations in the superconducting state is negligible.

The Knight shift of Sb can be deduced from the spectra splitting. The field calibrated

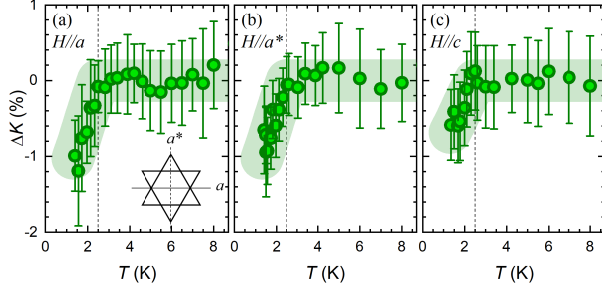


FIG. 3. Temperature dependence of ΔK of ^{121}Sb with (a) $H \parallel a$ (b) $H \parallel a^*$ and (c) $H \parallel c$, where a and a^* are orthogonal directions in the basal plane. The vertical dashed lines indicate the position of T_c .

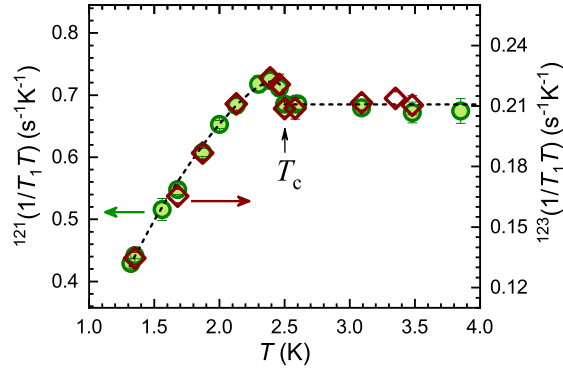


FIG. 4. Temperature dependence of $^{121}(1/T_1T)$ (left axis) and $^{123}(1/T_1T)$ (right axis). A Hebel-Slichter coherence peak appears just below T_c . The curve and line are guides to the eyes.

by a Gauss meter has an uncertainty, so the absolute Knight shift value is not reliable in an ultra-low field. The relative Knight shift $\Delta K = K - K_0$, where K_0 is the average value above T_c , has very weak dependence on field. The ΔK values for all directions are almost unchanged above T_c and decrease below T_c , as shown in Fig. 3, which is consistent with spin-singlet pairing. The perturbing field is much larger than the lower critical field, so the drop below T_c is not from Meissner effect but intrinsic spin susceptibility.

In an ultra-low field, ^{121}K measurements have large errors which preclude further analysis. On the other hand, spin-lattice relaxation rate can be measured accurately. $^{121/123}(1/T_1T)$ shows a clear Hebel-Slichter coherence peak just below T_c and then rapidly decreases at low temperatures as shown in Fig. 4. It evidences that the superconducting gap is of s-wave symmetry. As for d or p-wave, gap sign changes over the Fermi surface, which suppresses

a coherence peak. In iron-based superconductors, s^\pm -wave also changes gap sign between different Fermi surfaces and suppresses a coherence peak[37]. So far, the Hebel-Slichter coherence peak has only been observed in s-wave superconductors. Here the coherence peak is small, which may be due to residual EFG fluctuations[38] and/or a strong electron-phonon coupling[39]. In other s-wave superconductors, the coherence peaks of Sb are also very small, such as in YbSb_2 [40] and $\text{BaTi}_2\text{Sb}_2\text{O}$ [36]. A recent STM study has suggested the absence of sign-change in the superconducting order parameter[41]. Magnetic penetration depth measured by tunneling diode oscillator has shown a nodeless behavior[30]. These results are both consistent with the s-wave gap symmetry. There are also experimentally observed residual density of states in the superconducting state[25, 41], which may be due to the competition between superconductivity and CDW. Another s-wave superconductor $\text{Ta}_4\text{Pd}_3\text{Te}_{16}$ also has a CDW order coexisting with superconductivity and shows residual density of states in the superconducting state[42].

$^{121}(1/T_1T)$ is measured at the split peak due to the CDW transition and shows sudden changes at both T_{CDW} and T_c , which indicates that the superconductivity coexists with the CDW state. The coexistence of superconductivity and topological charge order may stimulate exotic excitations in the surface state[26, 43], which needs further investigations. Recently another superconducting phase at high pressure was found in CsV_3Sb_5 [24, 25]. Whether the high-pressure superconducting phase is the same as that at ambient pressure needs further studies.

In conclusion, we have performed ^{51}V NMR and $^{121/123}\text{Sb}$ NQR studies on CsV_3Sb_5 . The variation of the NMR and NQR spectra below T_{CDW} can be understood by the occurrence of a first-order commensurate CDW transition. EFG fluctuations are suppressed and magnetic fluctuations become dominant at low temperature. In the superconducting state, ^{121}K decreases and $^{121/123}(1/T_1T)$ shows a coherence peak just below T_c , which is the hallmark of the s-wave full gap superconductivity. The superconductivity coexists with the CDW state, which may lead to exotic surface state.

We thank S. K. Su, X. B. Zhou and B. Su for assistance in some of the measurements. This work was supported by the National Key Research and Development Program of China (Grant No. 2017YFA0302901, 2018YFE0202600, and 2016YFA0300504), the National Natural Science Foundation of China (Grant No. 11921004, 11634015, 11822412 and 11774423), the Beijing Natural Science Foundation (Grant No. Z200005), and the Strategic Priority

Research Program and Key Research Program of Frontier Sciences of the Chinese Academy of Sciences (Grant No. XDB33010100).

- [1] W.-S. Wang, Z.-Z. Li, Y.-Y. Xiang, and Q.-H. Wang, Competing electronic orders on kagome lattices at van Hove filling, *Phys. Rev. B* **87**, 115135 (2013).
- [2] M. L. Kiesel, C. Platt, and R. Thomale, Unconventional Fermi Surface Instabilities in the Kagome Hubbard Model, *Phys. Rev. Lett.* **110**, 126405 (2013).
- [3] S. Yan, D. A. Huse, and S. R. White, Spin-Liquid Ground State of the $S = 1/2$ Kagome Heisenberg Antiferromagnet, *Science* **332**, 1173 (2011).
- [4] M. Fu, T. Imai, T.-H. Han, and Y. S. Lee, Evidence for a gapped spin-liquid ground state in a kagome Heisenberg antiferromagnet, *Science* **350**, 655 (2015).
- [5] P. Khuntia, M. Velazquez, Q. Barthélemy, F. Bert, E. Kermarrec, A. Legros, B. Bernu, L. Messio, A. Zorko, and P. Mendels, Gapless ground state in the archetypal quantum kagome antiferromagnet $\text{ZnCu}_3(\text{OH})_6\text{Cl}_2$, *Nature Physics* **16**, 469 (2020).
- [6] H.-M. Guo and M. Franz, Topological insulator on the kagome lattice, *Phys. Rev. B* **80**, 113102 (2009).
- [7] W.-H. Ko, P. A. Lee, and X.-G. Wen, Doped kagome system as exotic superconductor, *Phys. Rev. B* **79**, 214502 (2009).
- [8] S.-L. Yu and J.-X. Li, Chiral superconducting phase and chiral spin-density-wave phase in a hubbard model on the kagome lattice, *Phys. Rev. B* **85**, 144402 (2012).
- [9] B. R. Ortiz, L. C. Gomes, J. R. Morey, M. Winiarski, M. Bordelon, J. S. Mangum, I. W. H. Oswald, J. A. Rodriguez-Rivera, J. R. Neilson, S. D. Wilson, E. Ertekin, T. M. McQueen, and E. S. Toberer, New kagome prototype materials: discovery of KV_3Sb_5 , RbV_3Sb_5 , and CsV_3Sb_5 , *Phys. Rev. Materials* **3**, 094407 (2019).
- [10] B. R. Ortiz, S. M. L. Teicher, Y. Hu, J. L. Zuo, P. M. Sarte, E. C. Schueller, A. M. M. Abeykoon, M. J. Krogstad, S. Rosenkranz, R. Osborn, R. Seshadri, L. Balents, J. He, and S. D. Wilson, CsV_3Sb_5 : A \mathbb{Z}_2 Topological Kagome Metal with a Superconducting Ground State, *Phys. Rev. Lett.* **125**, 247002 (2020).
- [11] B. R. Ortiz, P. M. Sarte, E. M. Kenney, M. J. Graf, S. M. L. Teicher, R. Seshadri, and S. D. Wilson, Superconductivity in the \mathbb{Z}_2 kagome metal KV_3Sb_5 ,

- Phys. Rev. Materials **5**, 034801 (2021).
- [12] Q. W. Yin, Z. J. Tu, C. S. Gong, Y. Fu, S. H. Yan, and H. C. Lei, Superconductivity and Normal-State Properties of Kagome Metal RbV_3Sb_5 Single Crystals, Chinese Physics Letters **38**, 6 (2021).
- [13] Y.-X. Jiang, J.-X. Yin, M. M. Denner, N. Shumiya, B. R. Ortiz, J. He, X. Liu, S. S. Zhang, G. Chang, I. Belopolski, Q. Zhang, M. S. Hossain, T. A. Cochran, D. Multer, M. Litskevich, Z.-J. Cheng, X. P. Yang, Z. Guguchia, G. Xu, Z. Wang, T. Neupert, S. D. Wilson, and M. Z. Hasan, Discovery of topological charge order in kagome superconductor KV_3Sb_5 (2020), arXiv:2012.15709 [cond-mat.supr-con].
- [14] S.-Y. Yang, Y. Wang, B. R. Ortiz, D. Liu, J. Gayles, E. Derunova, R. Gonzalez-Hernandez, L. Šmejkal, Y. Chen, S. S. P. Parkin, S. D. Wilson, E. S. Toberer, T. McQueen, and M. N. Ali, Giant, unconventional anomalous Hall effect in the metallic frustrated magnet candidate, KV_3Sb_5 , Science Advances **6**, eabb6003 (2020).
- [15] E. M. Kenney, B. R. Ortiz, C. Wang, S. D. Wilson, and M. J. Graf, Absence of local moments in the kagome metal KV_3Sb_5 as determined by muon spin spectroscopy, Journal of Physics: Condensed Matter **33**, 235801 (2021).
- [16] F. H. Yu, T. Wu, Z. Y. Wang, B. Lei, W. Z. Zhuo, J. J. Ying, and X. H. Chen, Concurrence of anomalous hall effect and charge density wave in a superconducting topological kagome metal (2021), arXiv:2102.10987 [cond-mat.str-el].
- [17] X. Feng, K. Jiang, Z. Wang, and J. Hu, Chiral flux phase in the Kagome superconductor AV_3Sb_5 , Science Bulletin <https://doi.org/10.1016/j.scib.2021.04.043> (2021).
- [18] M. M. Denner, R. Thomale, and T. Neupert, Analysis of charge order in the kagome metal AV_3Sb_5 ($A = \text{K, Rb, Cs}$) (2021), arXiv:2103.14045 [cond-mat.str-el].
- [19] H. X. Li, T. T. Zhang, Y. Y. Pai, C. Marvinney, A. Said, T. Yilmaz, Q. Yin, C. Gong, Z. Tu, E. Vescovo, R. G. Moore, S. Murakami, H. C. Lei, H. N. Lee, B. Lawrie, and H. Miao, Observation of Unconventional Charge Density Wave without Acoustic Phonon Anomaly in Kagome Superconductors AV_3Sb_5 ($A = \text{Rb, Cs}$) (2021), arXiv:2103.09769 [cond-mat.supr-con].
- [20] X. Zhou, Y. Li, X. Fan, J. Hao, Y. Dai, Z. Wang, Y. Yao, and H.-H. Wen, Origin of the Charge Density Wave in the Kagome Metal CsV_3Sb_5 as Revealed by Optical Spectroscopy (2021), arXiv:2104.01015 [cond-mat.supr-con].
- [21] K. Y. Chen, N. N. Wang, Q. W. Yin, Y. H. Gu, K. Jiang, Z. J. Tu, C. S. Gong, Y. Uwa-

- toko, J. P. Sun, H. C. Lei, J. P. Hu, and J.-G. Cheng, Double Superconducting Dome and Triple Enhancement of T_c in the Kagome Superconductor CsV_3Sb_5 under High Pressure, *Phys. Rev. Lett.* **126**, 247001 (2021).
- [22] F. Du, S. Luo, B. R. Ortiz, Y. Chen, W. Duan, D. Zhang, X. Lu, S. D. Wilson, Y. Song, and H. Yuan, Pressure-induced double superconducting domes and charge instability in the kagome metal KV_3Sb_5 , *Phys. Rev. B* **103**, L220504 (2021).
- [23] Z. Zhang, Z. Chen, Y. Zhou, Y. Yuan, S. Wang, J. Wang, H. Yang, C. An, L. Zhang, X. Zhu, Y. Zhou, X. Chen, J. Zhou, and Z. Yang, Pressure-induced reemergence of superconductivity in the topological kagome metal Cv_3sb_5 , *Phys. Rev. B* **103**, 224513 (2021).
- [24] X. Chen, X. Zhan, X. Wang, J. Deng, X.-B. Liu, X. Chen, J.-G. Guo, and X. Chen, Highly Robust Reentrant Superconductivity in CsV_3Sb_5 under Pressure, *Chinese Physics Letters* **38**, 057402 (2021).
- [25] C. C. Zhao, L. S. Wang, W. Xia, Q. W. Yin, J. M. Ni, Y. Y. Huang, C. P. Tu, Z. C. Tao, Z. J. Tu, C. S. Gong, H. C. Lei, Y. F. Guo, X. F. Yang, and S. Y. Li, Nodal superconductivity and superconducting domes in the topological Kagome metal CsV_3Sb_5 (2021), arXiv:2102.08356 [cond-mat.supr-con].
- [26] Z. Liang, X. Hou, W. Ma, F. Zhang, P. Wu, Z. Zhang, F. Yu, J. J. Ying, K. Jiang, L. Shan, Z. Wang, and X. H. Chen, Three-dimensional charge density wave and robust zero-bias conductance peak inside the superconducting vortex core of a kagome superconductor CsV_3Sb_5 (2021), arXiv:2103.04760 [cond-mat.supr-con].
- [27] H. Chen, H. Yang, B. Hu, Z. Zhao, J. Yuan, Y. Xing, G. Qian, Z. Huang, G. Li, Y. Ye, Q. Yin, C. Gong, Z. Tu, H. Lei, S. Ma, H. Zhang, S. Ni, H. Tan, C. Shen, X. Dong, B. Yan, Z. Wang, and H.-J. Gao, Roton pair density wave and unconventional strong-coupling superconductivity in a topological kagome metal (2021), arXiv:2103.09188 [cond-mat.supr-con].
- [28] Y. Wang, S. Yang, P. K. Sivakumar, B. R. Ortiz, S. M. L. Teicher, H. Wu, A. K. Srivastava, C. Garg, D. Liu, S. S. P. Parkin, E. S. Toberer, T. McQueen, S. D. Wilson, and M. N. Ali, Proximity-induced spin-triplet superconductivity and edge supercurrent in the topological Kagome metal, $\text{K}_{1-x}\text{V}_3\text{Sb}_5$ (2020), arXiv:2012.05898 [cond-mat.supr-con].
- [29] J.-P. Xu, M.-X. Wang, Z. L. Liu, J.-F. Ge, X. Yang, C. Liu, Z. A. Xu, D. Guan, C. L. Gao, D. Qian, Y. Liu, Q.-H. Wang, F.-C. Zhang, Q.-K. Xue, and J.-F. Jia, Experimental Detection of a Majorana Mode in the core of a Magnetic Vortex inside a Topological Insulator-

- Superconductor $\text{Bi}_2\text{Te}_3/\text{NbSe}_2$ Heterostructure, *Phys. Rev. Lett.* **114**, 017001 (2015).
- [30] W. Duan, Z. Nie, S. Luo, F. Yu, B. R. Ortiz, L. Yin, H. Su, F. Du, A. Wang, Y. Chen, X. Lu, J. Ying, S. D. Wilson, X. Chen, Y. Song, and H. Yuan, Nodeless superconductivity in the kagome metal CsV_3Sb_5 (2021), arXiv:2103.11796 [cond-mat.supr-con].
- [31] W. G. Clark, M. E. Hanson, F. Lefloch, and P. Ségransan, Magnetic resonance spectral reconstruction using frequency-shifted and summed Fourier transform processing, *Review of Scientific Instruments* **66**, 2453 (1995).
- [32] S. Ni, S. Ma, Y. Zhang, J. Yuan, H. Yang, Z. Lu, N. Wang, J. Sun, Z. Zhao, D. Li, S. Liu, H. Zhang, H. Chen, K. Jin, J. Cheng, L. Yu, F. Zhou, X. Dong, J. Hu, H.-J. Gao, and Z. Zhao, Anisotropic superconducting properties of kagome metal csv_3sb_5 , *Chinese Physics Letters* **38**, 057403 (2021).
- [33] A. Sakurai, M. Matsumura, H. Kato, T. Nishioka, E. Matsuoka, K. Hayashi, and T. Takabatake, Low-Field Knight Shift Measurement at Sb Site for Alkaline-Earth Filled Skutterudites $\text{AFe}_4\text{Sb}_{12}$ ($A = \text{Sr}$ and Ca), *Journal of the Physical Society of Japan* **77**, 063701 (2008).
- [34] K. Asayama, *NUCLEAR MAGNETIC RESONANCE IN ITINERANT ELECTRON SYSTEM* (SHOKABO, TOKYO, 2002).
- [35] M.-H. Julien, V. Simonet, B. Canals, R. Ballou, A. K. Hassan, M. Affronte, V. O. Garlea, C. Darie, and P. Bordet, Inhomogeneous magnetism in the doped kagome lattice of $\text{LaCuO}_{2.66}$, *Phys. Rev. B* **87**, 214423 (2013).
- [36] S. Kitagawa, K. Ishida, K. Nakano, T. Yajima, and H. Kageyama, s -wave superconductivity in superconducting $\text{BaTi}_2\text{Sb}_2\text{O}$ revealed by $^{121/123}\text{Sb}$ -NMR/nuclear quadrupole resonance measurements, *Phys. Rev. B* **87**, 060510(R) (2013).
- [37] D. Parker, O. V. Dolgov, M. M. Korshunov, A. A. Golubov, and I. I. Mazin, Extended s_{\pm} scenario for the nuclear spin-lattice relaxation rate in superconducting pnictides, *Phys. Rev. B* **78**, 134524 (2008).
- [38] Z. Li, W. H. Jiao, G. H. Cao, and G.-q. Zheng, Charge fluctuations and nodeless superconductivity in quasi-one-dimensional $\text{Ta}_4\text{Pd}_3\text{Te}_{16}$ revealed by ^{125}Te -NMR and ^{181}Ta -NQR, *Phys. Rev. B* **94**, 174511 (2016).
- [39] H. Kotegawa, K. Ishida, Y. Kitaoka, T. Muranaka, and J. Akimitsu, Evidence for Strong-Coupling s -Wave Superconductivity in MgB_2 : ^{11}B NMR Study, *Phys. Rev. Lett.* **87**, 127001 (2001).

- [40] Y. Kohori, T. Kohara, N. Sato, and T. Kinokiri, Sb NQR study of superconducting YbSb_2 , *Physica C: Superconductivity* **388-389**, 579 (2003), proceedings of the 23rd International Conference on Low Temperature Physics (LT23).
- [41] H.-S. Xu, Y.-J. Yan, R. Yin, W. Xia, S. Fang, Z. Chen, Y. Li, W. Yang, Y. Guo, and D.-L. Feng, Multiband superconductivity with sign-preserving order parameter in kagome superconductor CsV_3Sb_5 (2021), arXiv:2104.08810 [cond-mat.supr-con].
- [42] J. Pan, W. H. Jiao, X. C. Hong, Z. Zhang, L. P. He, P. L. Cai, J. Zhang, G. H. Cao, and S. Y. Li, Nodal superconductivity and superconducting dome in the layered superconductor $\text{Ta}_4\text{Pd}_3\text{Te}_{16}$, *Phys. Rev. B* **92**, 180505 (2015).
- [43] L. Fu and C. L. Kane, Superconducting proximity effect and majorana fermions at the surface of a topological insulator, *Phys. Rev. Lett.* **100**, 096407 (2008).